Modeling and Design Implications of Noncollocated Control in Flexible Systems

V. A. Spector
TRW Space and Defense,
Redondo Beach, CA 90278
and
University of Southern California,
Department of Mechanical Engineering,
Los Angeles, CA 90089-1453

H. Flashner
University of Southern California,
Department of Mechanical Engineering,
Los Angeles, CA 90089-1453

In this paper we investigate generic properties of structural modeling pertinent to structural control, with emphasis on noncollocated systems. Analysis is performed on a representative example of a pinned-free Euler-Bernoulli beam with distributed sensors. Analysis in the wave number plane highlights the crucial qualitative characteristics common to all structural systems. High sensitivity of the transfer function zeros to errors in model parameters and sensor locations is demonstrated. The existence of finite right half plane zeros in noncollocated systems, along with this high sensitivity, further complicates noncollocated controls design. A numerical method for accurate computation of the transfer function zeros is proposed. Wiener-Hopf factorization is used to compute equivalent delay time, which is important in controls design.

1 Introduction

One of the most important problems in control system design for large flexible structures is simultaneously achieving high performance and robustness. Since there is a trade-off between robustness and model accuracy, accurate modeling of the structure is essential to successful control system design [1], [2]. Most of the widely used methods of modeling structures rely heavily on modal analysis, which is in many cases inadequate for high performance control system development. Moreover, this type of analysis requires a form of modal truncation that can further degrade the accuracy of the plant model.

Most existing control design methods for flexible system, such as the Independent Modal Space Control (IMSC) [3], low-authority high-authority control design [4], frequency weighted LQG [5], and positivity [6], require modal truncation. With collocated actuators and sensors, modal truncation is usually not a significant factor in control design. This is because a collocated system with rate feedback is inherently stable, due to energy dissipation.

Noncollocated control systems, in contrast, lack these inherent stability characteristics. Here, inaccuracies resulting from model uncertainties and modal truncation present fundamental difficulties in both performance and stability. These limitations directly result from the fact that a noncollocated system is always nonminimum phase above some finite frequency. Nonminimum phase behavior is an inescapable result of the finite propagation speed of elastic deformation waves in the structure. Performance of nonminimum phase systems has inherent limitations; physical realizability requirements on the compensator impose definite restrictions on achievable closed loop characteristics [7]. Modeling inaccuracies can lead to qualitatively erroneous control designs by mismodeling a nonminimum phase system with a minimum phase model.

An adequate model of a noncollocated system must preserve both the qualitative and quantitative characteristics of both the poles and the zeros of the transfer function. Product series representation of the transfer function meets this need. The product series expansion has been used by Goodson [8] and Wie [9] as a more accurate alternative to the usual modal summation formulation. Wie [9] applied the product expansion method to the longitudinal vibration of a free-free bar and to the transverse vibration of a free-free beam. These results were compared with those obtained from the modal summation, revealing the inadequacy of modal summation. Reference [8] lists formulas for product expansions of several commonly occurring transcendental transfer functions. Jeffreys and Jeffreys [10] discusses the Mittag-Leffler product expanison theorem and derives some of the results used in [8].

In this paper, we study the characteristics of flexible structure control with an emphasis on systems with noncollocated sensors and actuators. Properties of general structural control systems are described in Section 2. Section 3 introduces an example of an Euler-Bernoulli beam that will provide a concrete demonstration of the generic properties discussed in Section 2. Section 3 contains detailed results for pole locations and the location of the zeros as a function of actuator/sensor separation. In Section 4, the results of the previous section are mapped into the s-plane for controls analysis purposes. Section 5 discusses the relation between the nonminimum phase right half plane zeros and the propagation delay time from actuator to sensor. Implications for structural control are discussed in Section 6. An Appendix contains a detailed derivation of the transfer function for the pinned-free beam example.

2 Properties of Flexible Structures

Control of flexible structures is complicated by the

Contributed by the Dynamic Systems and Control Division for publication in the JOURNAL OF DYNAMIC SYSTEMS, MEASUREMENT, AND CONTROL. Manuscript received by the Dynamic Systems and Control Division November 17, 1987; revised manuscript received July 15, 1988. Associate Editor: A. G. Ulsoy.

distributed parameter nature of the system. This leads to a plant model that can be represented by an infinite sum of lightly damped, closely spaced, vibrational models. This infinite dimensional plant needs to be controlled by a finite dimensional controller. Design analysis methods for finite dimensional controllers require finite dimensional plant models and, therefore, truncation of the original model. In flexible structure control design, truncation results in the well known phenomena of control and observation spillover [1].

For high accuracy control, the closed loop system requires a high bandwidth for command tracking and disturbance rejection. As a result, the truncated model contains a finite, but large, number of lightly damped modes. Close spacing of the modal frequencies, coupled with the high uncertainties present in structural modeling, presents significant difficulties in control design. Model uncertainties result not only from structural parameter uncertainties, but also from the typically ill-defined boundary conditions and the choice of the underlying structural theory and methodology. The various structural theories such as Euler-Bernoulli beam theory, Timoshenko beam theory, and general three-dimensional elasticity theory provide a trade-off between accuracy and ease of analysis. A similar trade-off exists between the candidate methodologies, such as partial differential equations, finite elements, and modal synthesis. At the system level, additional model uncertainties arise from poorly defined disturbance sources and their locations on the structure.

The above uncertainties place stringent robustness requirements on the control system. A frequently used approach to ensuring a certain degree of robustness is to collocate the sensors and actuators, resulting in an energy dissipating configuration [6]. However, because of physical placement and hardware limitations, this approach is often impossible. Moreover, collocation does not always result in the required high level of performance.

To provide a concrete example of a noncollocated control system, we chose the example of a pinned-free beam with a torquer actuator at the pinned end and sensors at arbitrary locations. This configuration is representative of a robot manipulator link and also possesses the essential properties of general flexible structure control problems. Specifically, it is a distributed parameter system with lightly damped and closely spaced vibrational modes. Selection of this example is also based on the fact that it can be solved analytically in closed form. Thus the sensitivity to modeling inaccuracies can be easily quantified and the implications of noncollocation can be expressed explicitly.

3 Beam Analysis in Wave Number Plane

In this section we analyze a pinned-free Euler-Bernoulli beam in the wave number plane. The transfer function from the actuator to sensors located along the beam is expressed using product expansions. The section concludes with a discussion of the effect of noncollocation on the relation between the transfer function poles and zeros.

Consider the pinned-free Euler-Bernoulli beam shown in Fig. 1. The beam has length L, Young's modulus E, area moment of inertia I, mass density per unit volume ρ, and cross-sectional area A. The input (actuator) is a torquer at the pinned end, $M(0, t)$, while the output (sensor) is the total deflection at an arbitrary point x along the beam, $y(x, t)$. It is assumed that both the rigid body and flexible body motions are small. The beam satisfies the partial differential equation [11]:

$$EI\frac{\partial^4 y(x,t)}{\partial x^4}+\rho A\frac{\partial^2 y(x,t)}{\partial t^2}=0 \tag{1}$$

along with the boundary conditions at the pinned end:

$$y(0,t)=0 \tag{2}$$

$$EI\frac{\partial^2 y(0,t)}{\partial x^2}=-M(0,t) \tag{3}$$

and at the free end:

$$EI\frac{\partial^2 y(L,t)}{\partial x^2}=0 \tag{4}$$

$$EI\frac{\partial^3 y(L,t)}{\partial x^3}=0 \tag{5}$$

The initial conditions are assumed to be zero, i.e., $y(x, 0)=0$ and $\dot{y}(x, 0)=0$. Equation (1) can be expressed more compactly by defining:

$$\beta^4=-\rho A/EI \tag{6}$$

and substituting to get:

$$\frac{\partial^4 y(x,t)}{\partial x^4}-\beta^4\frac{\partial^2 y(x,t)}{\partial t^2}=0 \tag{7}$$

The general solution to this problem can be found by taking the Laplace transform with respect to time. The resulting ordinary differential equation for the transform $Y(x, s)$ has the algebraic characteristic equation:

$$p^4-\beta^4 s^2=0 \tag{8}$$

where s is the complex temporal frequency. The parameter p can be interpreted as a spatial frequency, $p=ik$ where k is the wave number and $i=\sqrt{-1}$. Note that equation (8) can be obtained by assuming a wave solution of the form:

$$y(x,t)=Ae^{(px+st)}$$

where p and s have the interpretations given above [11].

In the Appendix, the characteristic roots of equation (8) are found and the boundary conditions are applied. This yields the transcendental transfer function from the torquer at $x=0$ to the displacement at a general point x, $0\le x\le L$:

$$G(x,\gamma)=Y(x,\gamma)/M(0,s)=N(x,\gamma)/D(\gamma) \tag{9}$$

where:

$$\gamma=\beta s^{1/2}=p_1 \tag{10}$$

is the first quadrant root of equation (8).
The numerator and denominator are:

$$N(x,\gamma)=a_1(\gamma)f_1(x,\gamma)+a_2(\gamma)f_2(x,\gamma)+a_3(\gamma)f_3(x,\gamma) \tag{11}$$

$$D(\gamma)=2EI\gamma^2 a_3(\gamma) \tag{12}$$

where the $a_n(\gamma)$ and $f_n(x, \gamma)$ are defined in the Appendix.

Equation (9) expresses the system transfer function as the ratio the numerator, equation (11), and the denominator, equation (12). Note that the numerator, which defines the zeros of the transfer function, depends on the sensor position x, while the denominator, which defines the poles (modal frequencies), does not. It is therefore only the zeros, and not the poles, that vary with sensor location. In particular, only the pattern of the zeros determines whether the system can be considered collocated for control purposes.

It is easy to verify that the four-way symmetry noted in the p-plane in equation (A2) carries over to the γ-plane. Hence, if γ is a root (of the numerator or denominator) then so are $-\gamma$, $i\gamma$, and $-i\gamma$. This property allows the search for roots (poles or zeros) to be restricted to the first quadrant in the γ-plane. In the following, the denominator and numerator roots will be found using product expansion techniques.

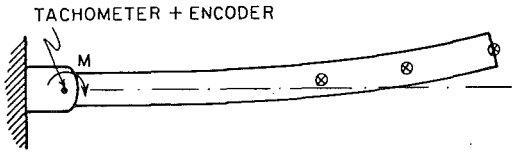

Fig. 1 Pinned-free beam model

3.1 Denominator Expansion. Factoring the denominator, equation (12), is relatively straightforward once a factoring of $a_3(\gamma)$, equation (A14), is found. It can be easily shown that $\gamma=0$ is a triple root of $a_3(\gamma)=0$. The resulting lead term of the product expansion is:

$$\frac{\partial^3 a_3(0)}{\partial\gamma^3}\frac{\gamma^3}{3!}=\frac{-2L^3\gamma^3}{3}. \tag{13}$$

The other roots of $a_3(\gamma)=0$ are defined implicitly by the roots of the transcendental equation:

$$\tan d_n=\tanh d_n \tag{14}$$

The four way symmetry noted above allows the search for roots of equation (14) to be limited to real positive values. In solving equation (14) numerically, it is also helpful to note that the higher roots differ by almost exactly π.

To each real positive root d_n of equation (14) there are four roots to the original equation $a_3(\gamma)=0$:

$$p_1=\quad\gamma=\quad+\ d_n/L \tag{15a}$$
$$p_2=\quad i\gamma=+i\ d_n/L \tag{15b}$$
$$p_3=-\quad\gamma=\quad-\ d_n/L \tag{15c}$$
$$p_4=-i\ \gamma=-i\ d_n/L \tag{15d}$$

Combining these roots gives for each real positive d_n a factor in the infinite product expansion:

$$(1-\gamma L/d_n)(1-i\gamma L/d_n)(1+\gamma L/d_n)(1+i\gamma L/d_n)$$
$$=(1-\gamma^4L^4/d_n^4) \tag{16}$$

In equation (16), the factors are normalized to unity for $\gamma=0$. Equations (13) and (16) then give the factored form of the denominator:

$$D(\gamma)=-(4/3)\mathrm{E}I\gamma^5L^3\prod_{n=1}^{\infty}(1-\gamma^4L^4/d_n^4) \tag{17a}$$

where:

$$\tan d_n=\tanh d_n \qquad \text{with } d_n>0, \text{ real} \tag{17b}$$

Since controls analysis is usually performed in the s-plane, the s-plane roots are of interest. By using equations (6), (8), and (10), each γ-plane quadruple maps into a complex conjugate pair of imaginary poles in the s-plane:

$$s_n=\pm i(\mathrm{E}I/\rho A)^{1/2}(d_n/L)^2 \tag{18}$$

Note that, as mentioned before, the poles of the transfer function do not depend on the actuator or sensor locations.

3.2 Numerator Expansion. Analytically factoring the numerator, equation (11), presents greater difficulty, except in the special cases $x=0$ and $x=L$. The problem arises because there are now two families of quadruples, with the solutions jumping abruptly from one family to the other as x is varied. The two families are defined by the p-plane quadruples:

$$Q_1=\{\alpha,\ -\alpha,\ i\alpha,\ -i\alpha\} \tag{19}$$

$$Q_2=\{\alpha(1+i),\ -\alpha(1+i),\ \alpha(1-i),\ -\alpha(1-i)\} \tag{20}$$

where α is real and positive. Quadruple Q_1 maps into a conjugate pair of purely imaginary zeros, while Q_2 maps into a pair of real zeros, one in the left half plane and the other in the right half plane (see Fig. 2).

3.2.1 Sensor at $x=0$. For $x=0$, the numerator is identically zero. However, the transfer function zeros can be found, by a limiting process as x approaches zero, from the roots of:

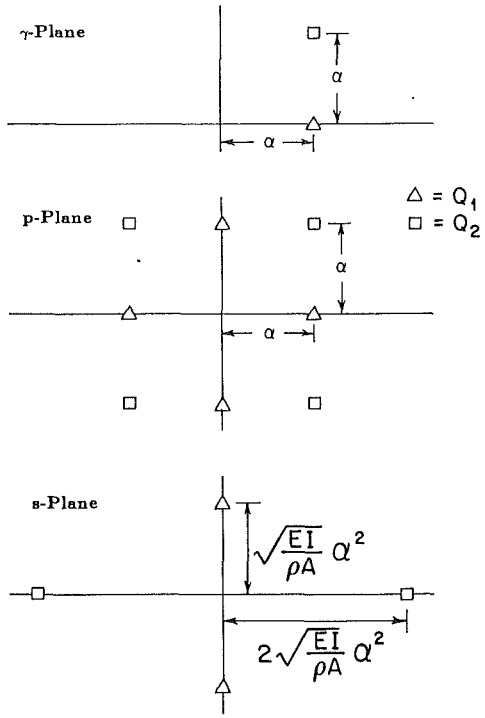

Fig. 2 Mappings between γ-, p-, and s-planes

$$1+\cos\gamma L\cosh\gamma L=0 \tag{21}$$

This can be factored ([8]) as:

$$2\sum_{n=1}^{\infty}(1-\gamma^4L^4/b_n^4) \tag{22a}$$

where:

$$1+\cos b_n\cosh b_n=0\ \ b_n>0, \text{ real} \tag{22b}$$

The factors in equation (22) map into pure imaginary conjugate pairs in the s-plane.

3.2.2. Sensor at $x=L$. For $x=L$, the numerator reduces to:

$$N(L,\gamma)=2(\sin\gamma L+\sinh\gamma L) \tag{23}$$

which can be factored ([8], [9]) as:

$$N(L,\gamma)=4\gamma L\sum_{n=1}^{\infty}(1+\gamma^4L^4/4c_n^4) \tag{24a}$$

where:

$$\tan c_n+\tanh c_n=0,\ c_n>0, \text{ real} \tag{24b}$$

The factors in equation (24) map into pairs of real zeros in the s-plane, with one of each pair in the left half plane and the other in the right half plane. Note that for this case the resulting transfer function is always nonminimum phase.

3.2.3 Sensor at General Point. For a general point x, $0<x<L$, the s-plane zeros will be a mixture of real and imaginary pairs. The pattern of the zeros, that is whether they are real or imaginary, is critical for control system design for flexible structures, since it determines whether the system is nonminimum phase. For the general case, numerical methods are required to determine the transfer function zeros. The four way symmetry allows the zeros to be determined numerically by one-dimensional searches along two half-lines. These searches can be performed either in the γ-plane along the

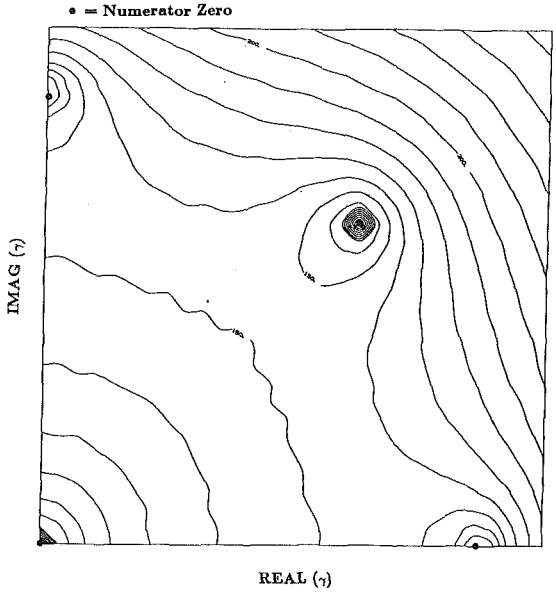

Fig. 3 Contour map of magnitude of numerator for $\eta = 0.8$

positive real axis and the first quadrant diagonal; or in the s-plane along the positive real and positive imaginary axes. Figure 3 depicts the magnitude of the numerator in the γ-plane for $x/L = 0.8$. Placement of the roots along the real (and imaginary) axis and the diagonal is clearly shown.

For a fixed value of $\eta = x/L$, the first ten transfer function zeros were determined numerically by evaluating the magnitude of the numerator, equation (11), along the following two half lines in the γ-plane:

$$\gamma = \alpha \tag{25a}$$

$$\gamma = \alpha(1 + i) \tag{25b}$$

where the parameter α is real and positive.

Figure 4 shows a composite plot of the roots in the γ-plane as η is varied from 0 to 1. Curves labeled "$i1$" to "$i10$" correspond to roots of the type of equation (25a). These roots map into a conjugate pair of pure imaginary s-plane zeros:

$$s = \pm i(EI/\rho A)^{1/2}\alpha^2 \tag{26}$$

Curves labeled "$r1$" to "$r10$" correspond to the second type of root, equation (25b). These map into a pair of real s-plane zeros:

$$s = \pm 2(EI/\rho A)^{1/2}\alpha^2 \tag{27}$$

For $\eta = 0$, only the "i" curves exist and the values of the γ-plane roots (small squares in Fig. 4) agree with the roots of the product expansion given by equation (22). For $\eta = 1$, only the "r" curves exist and the values of the γ-plane roots (small circles in Fig. 4) agree with the roots of the product expansion given by equation (24).

Note that in the "r" curve case, one of the zeros is in the right half s-plane, resulting in a nonminimum phase transfer function. For any given value of η the sum of the number of "i" curves and "r" curves in Fig. 4 is exactly ten. However, as η increases, the number of "r" curves increases and the number of "i" curves decreases. This means that the number of low frequency right half plane zeros increases as the actuator/sensor separation increases, as shown in Fig. 5. Figures 4 and 5 show that the nth mode will have a right half plane zero associated with it if the normalized sensor/actuator separation η is greater than approximately $1/n$. This approximation improves as the flexible mode number n increases.

As shown in Fig. 4, the "i" curves intersect precisely at the nodes of each of the modes at the corresponding modal frequency (small triangles in Fig. 4). The intersection of the "i"

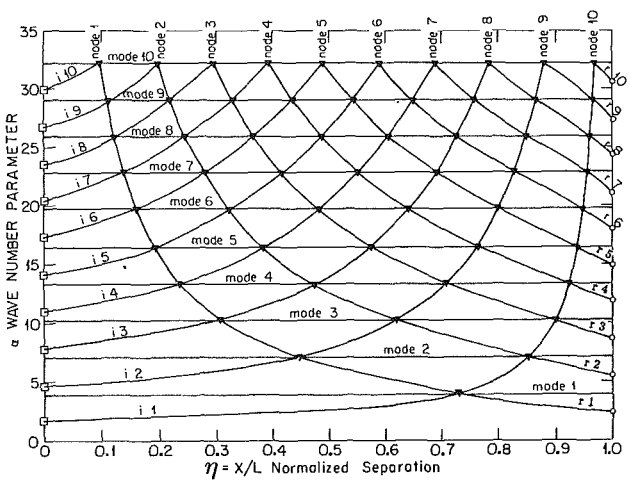

Fig. 4 Interrelation among γ-plane modes, nodes, and zeros

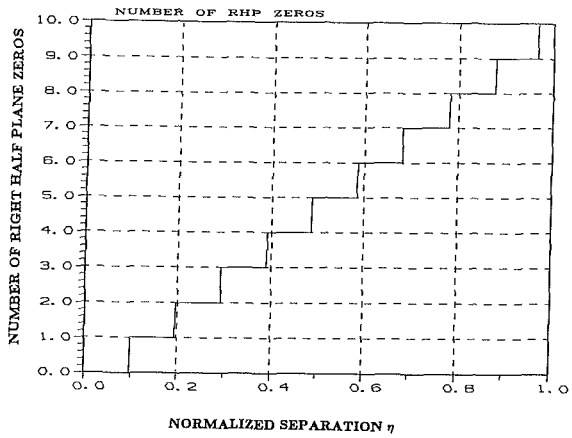

Fig. 5 Number of right half plane zeros related to first ten modes

curves with the modal frequencies at the nodal points results from the fact that a node occurs whenever an imaginary axis zero cancels an imaginary axis pole. While the "r" curves do not precisely intersect with the "i" curves at the nodal points, the error is generally less than 1 percent.

The above facts allow the approximate determination of the zero locations as a function of η using finite set of modes and their corresponding nodes. Modal frequencies and nodal locations can be determined using standard modal analysis techniques. The "r" and "i" curves can the be constructed by interpolating between the resulting points in the $\alpha - \eta$ plane. For the case in Fig. 4, interpolation is aided by analytical expressions for the zeros at $\eta = 0$ and $\eta = 1$. This procedure provides a method of performing an approximate product series expansion of the numerator using only data on the modal frequencies and nodal locations. The resulting zeros will not suffer from the numerical inaccuracy of the truncated modal summation approach.

4 Pole/Zero Pattern in s-Plane

As mentioned previously, control analysis is performed in the s-plane. Using equations (26) and (27), the s-plane zeros were computed for various values of normalized separation η. The symmetry of the pole/zero distribution with respect to both the real and imaginary axes allows attention to be resticted to the first quadrant. Figures (6a) to (6c) show the first quadrant pole/zero configuration for $\eta = 0.7$, 0.75, and 0.8 in terms of normalized s-plane frequency $w = i\,\Omega = s/|\beta|^2 L^2$. The figures show two poles at the origin, representing the rigid body pinned mode, and six conjugate imaginary pairs of poles representing the first six flexible body

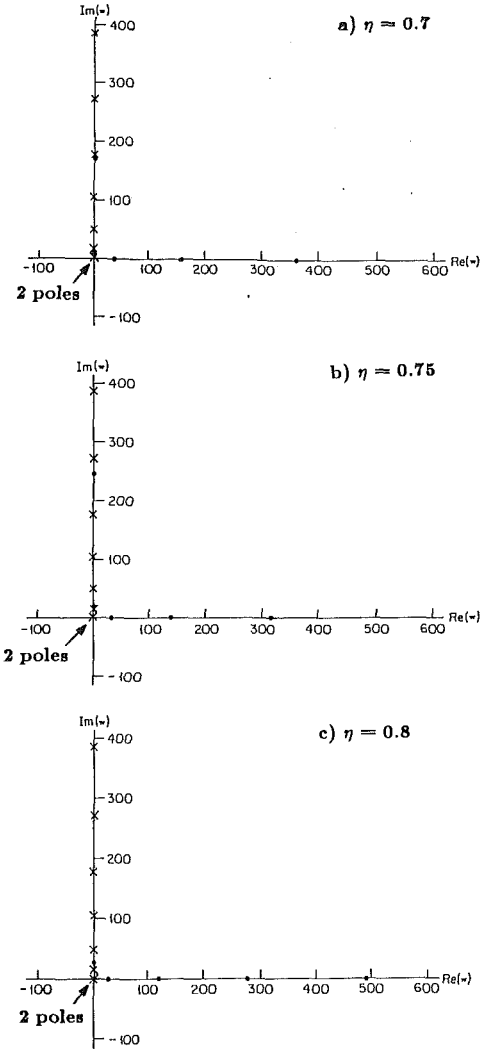

Fig. 6 First quadrant pole/zero configuration

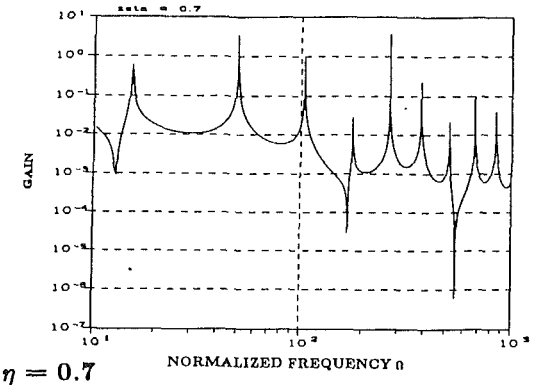

a) $\eta = 0.7$

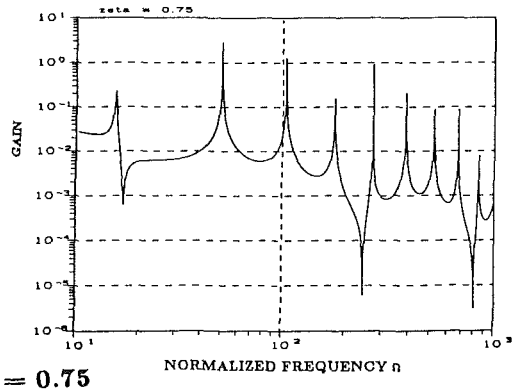

b) $\eta = 0.75$

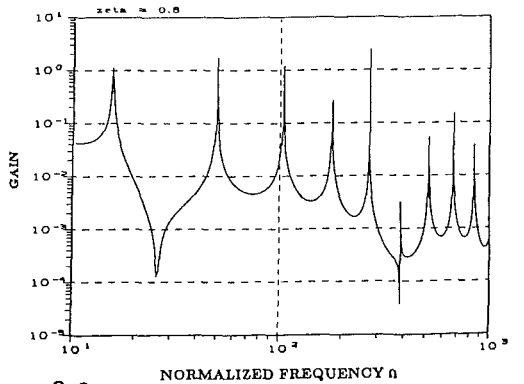

c) $\eta = 0.8$

Fig. 7 Torquer to displacement transfer function: gain

modes. Note that as η increases from 0.7 to 0.75, the two imaginary zeros shown cross the first and fourth flexible mode poles, respectively. As η increase from 0.75 to 0.8, one of the imaginary zeros goes off scale and an additional zero appears on the real axis. In general, as η increases, the imaginary zeros increase in frequency until they disappear completely for $\eta = 1$. The real zeros move in a complementary manner, being entirely absent for $\eta = 0$ and then appearing at progressively lower frequencies as η increases.

Figures 7(*a*) to 7(*c*) show the transfer function gains as a function of the normalized frequency Ω for $\eta = 0.7$, 0.75, and 0.8, while the corresponding phases are shown in Fig. 8(*a*) to 8(*c*). It is apparent that the system behavior is qualitatively different for each sensor location, especially at low frequencies. This change in behavior can be traced to the interchanges of the pole/zero sequences along the imaginary axis as shown in Fig. 6.

As η increases, the sensor location eventually reaches, and then crosses, a nodal point of a given mode, thereby interchanging the pole/zero sequence. This pole/zero interchange phenomenon has been previously noted by Rosenthal [12]. When the sensor is located exactly at a node, pole/zero cancellation occurs and the transfer function does not reveal the existence of the mode. For small differences between the sensor and node locations, the transfer function gain and phase is very sensitive to both frequency and sensor location. In particular, consider the node of the first flexible mode ($\Omega = 15.418$) located at $\eta = 0.74$. As shown in Fig. 8, the transfer function phase at given frequencies near the first flexible mode differs by up to 360 degrees between the three cases $\eta = 0.7$, 0.75, and 0.8.

5 Delay Time of Noncollocated Systems

An important, but often neglected, feature of noncollocated structure control is the delay time resulting from finite wave propagation velocity. Time delay manifests itself in the frequency domain as an accumulation of negative phase for increasing frequency. For a pure (nondispersive) time delay, the relation between the phase ϕ, the circular frequency ω, and the delay time T is given by:

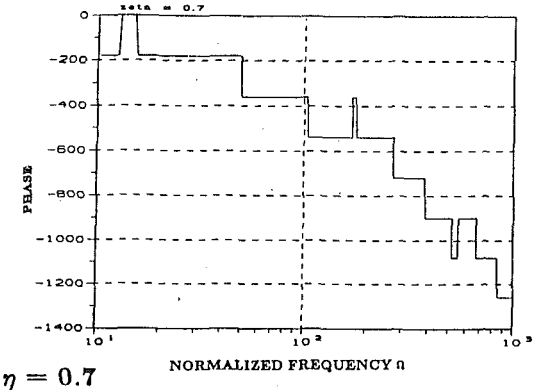

a) $\eta = 0.7$

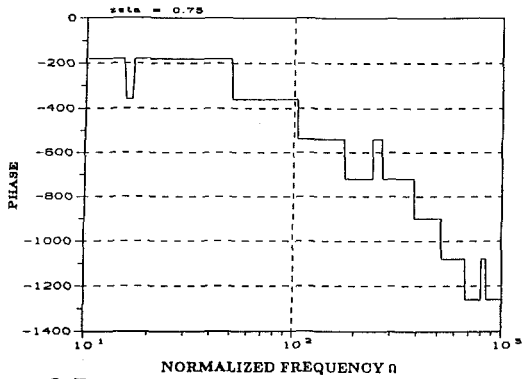

b) $\eta = 0.75$

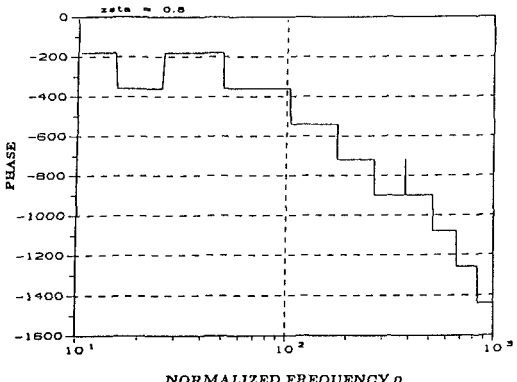

c) $\eta = 0.8$

Fig. 8 Torquer to displacement transfer function: phase

$$\phi_{\text{delay}}(\omega) = -\omega T \tag{28}$$

Since wave propagation in beams is dispersive [11], the propagation velocity, and thus the delay, is frequency dependent. Equation (28) can still be used to define an equivalent delay time at any given frequency.

The additional phase lag resulting from a time delay directly reduces the system phase margin. If the phase lag from the time delay exceeds the system phase margin at the cross-over frequency, system instability will result. Exact compensation for a time delay requires a physically unrealizable anticipatory compensator. Practical compensators can seldom achieve even 180 degrees of lead (positive phase) due to such factors as noise and saturation. The fact that the negative phase accumulation of a noncollocated flexible system, resulting from propagation delay, is unbounded therefore limits the achievable closed-loop bandwidth.

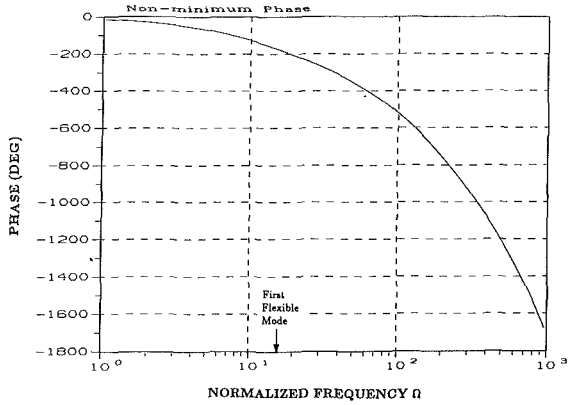

Fig. 9 Nonminimum phase factor of transfer function to $\eta = 1$

The product expansion approach allows an accurate determination of the phase, and thus of the delay. For a collocated system, poles and zeros alternate on the imaginary axis, resulting in a phase contribution from the flexible modes no more negative than -180 degrees. As noted in the previous sections, noncollocated systems do not have alternating imaginary poles and zeros, resulting in accumulation of negative phase from flexible modes beyond -180 degrees. Noncollocated systems have a mixture of imaginary and real zeros, with half the real zeros in the right half plane. Transfer functions for noncollocated systems are thus always nonminimum phase beyond some finite frequency.

Wiener-Hopf spectral factorization [7] can be used to compute the extra phase resulting from the nonminimum phase characteristic. Since the uncontrolled structure is always stable, none of the transfer function poles are in the open right half plane. The transfer function can therefore be factored as:

$$G(x, s) = \frac{[N(x, s)]^- [N(x, s)]^+}{D(s)}$$

$$= \left\{\frac{[N(x, s)]^- [N(x, -s)]^+}{D(s)}\right\} \cdot \left\{\frac{[N(x, s)]^+}{[N(x, -s)]^+}\right\} \tag{29}$$

$$= G_{mp}(x, s) G_{nmp}(x, s)$$

where $[\,]^+$ contains factors with roots in the open right half plane and $[\,]^-$ contains factors with roots in the closed left half plane. The first factor in equation (29), $G_{mp}(x, s)$, contains the minimum phase part of the transfer function and has the same gain as the original transfer function $G(x, s)$. The second factor, $G_{nmp}(x, s)$, has unity gain at all frequencies and contains all of the excess negative phase due to the nonminimum phase character of the original transfer function. Use of the product series expansion allows the factoring in equation (29) to be performed by inspection.

For the pinned-free beam example, with $\eta = 1$ ($x = L$), the nonminimum phase factor can be found, in terms of normalized frequency w, from equation (24*a*) as:

$$G_{nmp}(L, w) = \prod_{n=1}^{\infty} \frac{(1 - w/2c_n^2)}{(1 + w/2c_n^2)} \tag{30}$$

where c_n is as in equation (24*b*). The phase of this factor, in terms of normalized frequency $w = i\Omega$, is:

$$\phi_{nmp}(i\Omega) = -2 \sum_{n=1}^{\infty} \tan^{-1}(\Omega/2c_n^2) \tag{31}$$

Figure 9 shows the nonminimum phase contribution for this

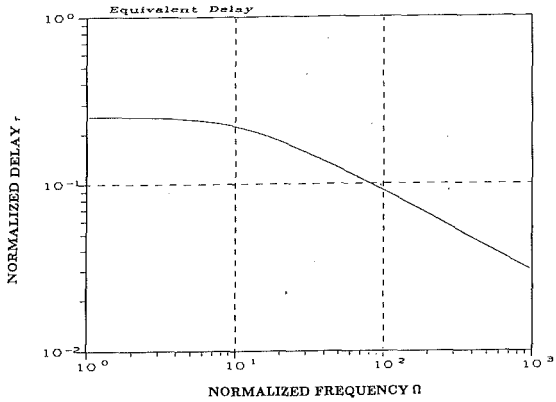

Fig. 10 Equivalent delay of nonminimum phase factor

case. Note that the nonminimum phase contribution is approximately -180 degrees at the first modal frequency, and increases rapidly thereafter. Due to sensor noise and other hardware considerations, it is seldom practical to add even as much as 180 degrees of lead compensation. Stabilizing this system with a bandwidth beyond the first flexible mode, using only a noncollocated (end-mounted) sensor, is therefore not realistic.

Figure 10 shows the equivalent delay time resulting from the nonminimum phase characteristic. The delay time is normalized as $\tau = |\beta|^2 L^2 T$, where T is the delay time in seconds. The continued decrease in delay time with frequency, approaching zero at very high frequencies, results from the simplifying assumptions of the Euler-Bernoulli model. The more accurate Timoshenko beam model predicts a nonzero high frequency asymptote for the equivalent delay time [13]. However, as shown in [13], the Euler-Bernoulli and Timoshenko models predict virtually identical delay times at low frequencies. Therefore, the Euler-Bernoulli model is suitable for predicting delay at low frequencies.

6 Implications for Structural Control

The example treated here has the generic properties of more complex structural control problems. Therefore the analysis presented here leads to the following general observations:

1) Accurate dynamic modeling of the structure is of critical importance is noncollocated structural control design. Small inaccuracies in the model can lead to qualitatively different system characteristics, resulting in deficient and possibly unstable designs. In particular, small variations in sensor locations can result in interchanging the ordering of poles and zeros, producing phase errors of up to -360 degrees. A phase error of this size virtually guarantees closed loop instability.

2) Noncollocated structural control systems are always nonminimum phase above some finite frequency. If this frequency is less than a decade above the control bandwidth, the additional negative phase severely constrains the achievable control system performance. The frequency at which the transfer function becomes nonminimum phase decreases as the sensor/actuator distance increases. A conventional modal model, that is perfectly adequate for collocated control design, may therefore be completely unsuitable for noncollocated control design. Increasing the control system bandwidth requirement can also necessitate a modeling technique that can more accurately determine the transfer function zeros.

3) Accurate modeling of the zeros within or near the control system bandwidth is a critical factor in structural control modeling. This issue, equally as important as other structural control concerns like control and observation spillover, has not been given appropriate attention.

Acknowledgment

The authors would like to thank Joanne Maguire, Ralph Iwens, and Frank Tung of TRW and Professor Firdaus Udwadia of USC for numerous helpful comments and suggestions on this paper.

References

1 Iwens, R. P., "Active Structural Control for Large Flexible Space Systems," EASCON 1981, Nov. 17-19, 1981.

2 Croopnick, S. R., Lin, Y. H., and Strunce, R. R., "A Survey of Automatic Control Techniques for Large Space Structures," VIII IFAC Symposium on Automatic Control in Space, Oxford, U. K., July 1979.

3 Meirovitch, L., and Baruh, H., "Control of Self Adjoint Distributed Systems," *AIAA Journal of Guidance and Control*, Vol. 5, Jan.-Feb. 1982, pp. 60-66.

4 Aubrun, J. N., Gupta, N. K., Lyons, M. G., and Margulies, G., "Large Space Structures Control: An Integrated Approach," AIAA Paper 79-1764, AIAA Guidance and Control Conference, Boulder, Colorado, August 1979.

5 Gupta, N. K., "Frequency-Shaped Cost Functionals: Extension of Linear-Quadratic-Gaussian Design Methods," *AIAA Journal of Guidance and Control*, Vol. 3, No. 6, Nov.-Dec. 1980.

6 Benhabib, R. J., Iwens, R. P., and Jackson, R. L., "Stability of Large Space Structure Control Systems Using Positivity Concepts," *AIAA Journal of Guidance and Control*, Vol. 4, No. 5, Sept.-Oct. 1981.

7 Newton, G. C., Gould, L. A., and Kaiser, J. F., *Analytical Design of Linear Feedback Controls*, Wiley, New York, 1957.

8 Goodson, R. E., "Distributed System Simulation Using Infinite Product Expansions," *Simulation*, Dec. 1970, pp. 255-263.

9 Wie, B., "On the Modeling and Control of Flexible Space Structures," SUDAAR 525, Stanford University Guidance and Control Laboratory, June 1981.

10 Jeffreys, H., and Jeffreys, B. S., *Method of Mathematical Physics*, Cambridge University Press, Cambridge, Third Edition, 1956, pp. 383-386.

11 Graff, K. F., *Wave Motion in Elastic Solids*, Ohio State University Press, 1975.

12 Rosenthal, D. E., "Experiments in Control of Flexible Structures with Uncertain Parameters," SUDAAR 542, Stanford University Guidance and Control Laboratory, Mar. 1984.

13 Spector, V. A., and Flashner, H., "Flexible Manipulator Modeling for Control System Development," AIAA Paper 87-2264, AIAA Guidance, Navigation and Control Conference, Monterey, Calif., Aug. 17-19, 1987.

APPENDIX

Pinned-Free Beam Transfer Function

This Appendix contains the detailed derivation of the transcendental transfer function for the pinned-free beam example.

The characteristic equation for the Euler-Bernoulli beam, equation (8), is easily factored into linear factors in terms of p, with s as a parameter:

$$(p-p_1)(p-p_2)(p-p_3)(p-p_4)=0 \tag{A1}$$

The characteristic values p_i, $i=1, 2, 3, 4$, are the roots of equation (8):

$$p_1 = +\beta s^{1/2} = \gamma \tag{A2a}$$
$$p_2 = +i\beta s^{1/2} = i\gamma \tag{A2b}$$
$$p_3 = -\beta s^{1/2} = -\gamma \tag{A2c}$$
$$p_4 = -i\beta s^{1/2} = -i\gamma \tag{A2d}$$

where the principal value is taken for the square root of the complex number s and:

$$\gamma = p_1 = \beta s^{1/2} \tag{A3}$$

Note that the four roots in equation (A2) are symmetrically placed in the p-plane.

The resulting solution is:

$$Y(x,s) = A_1(s)e^{p_1 x} + A_2(s)e^{p_2 x} + A_3(s)e^{p_3 x} + A_4(s)e^{p_4 x} \tag{A4}$$

where the A_i, $i=1, 2, 3, 4$ are functions of s to be determined from the boundary conditions. However, equation (A4) ex-

plicitly contains the total spatial dependence of the transfer function.

Using trigonometric and hyperbolic functions, equation (A4) can be written in a more convenient form in terms of the single parameter γ.

$$Y(x, \gamma) = C_1(\gamma)\sin\gamma x + C_2(\gamma)\cos\gamma x + C_3(\gamma)\sinh\gamma x + C_4(\gamma)\cosh\gamma x \quad \text{(A5)}$$

The coefficients C_i, $i = 1, 2, 3, 4$, in equation (A5) are found by applying the time transforms of the boundary conditions, derived from equations (2) to (5). The boundary conditions at $x = 0$ result in:

$$C_2(\gamma) = M(0, s)/2EI\gamma^2 \quad \text{(A6)}$$

$$C_4(\gamma) = -C_2(\gamma) \quad \text{(A7)}$$

$M(0, s)$ is the Laplace transform of the applied moment at $x = 0$, $M(0, t)$, and is evaluated at $s = \gamma^2/\beta^2$. Applying the boundary conditions at $x = L$ and solving the two resulting simultaneous equations gives:

$$\begin{bmatrix} C_1(\gamma) \\ C_3(\gamma) \end{bmatrix} = \frac{M(0, s)}{2EI\gamma^2(\cos\gamma L\sinh\gamma L - \sin\gamma L\cosh\gamma L)} \cdot \begin{bmatrix} 1 + \cos\gamma L\cosh\gamma L + \sin\gamma L\sinh\gamma L \\ 1 + \cos\gamma L\cosh\gamma L - \sin\gamma L\sinh\gamma L \end{bmatrix} \quad \text{(A8)}$$

Equations (A5) to (A8) can now be combined and placed over a common denominator. The final result is the transcendental transfer function from the torquer at $x = 0$ to the displacement at a general point x, $0 \le x \le L$:

$$G(x, \gamma) = Y(x, \gamma)/M(0, s) = N(x, \gamma)/D(\gamma) \quad \text{(A9)}$$

Here, the numerator and denominator are:

$$N(x, \gamma) = a_1(\gamma)f_1(x, \gamma) + a_2(\gamma)f_2(x, \gamma) + a_3(\gamma)f_3(x, \gamma) \quad \text{(A10)}$$

$$D(\gamma) = 2EI\gamma^2 a_3(\gamma) \quad \text{(A11)}$$

The position-independent terms in equations (A10) and (A11) are:

$$a_1(\gamma) = 1 + \cos\gamma L\cosh\gamma L \quad \text{(A12)}$$

$$a_2(\gamma) = \sin\gamma L\sinh\gamma L \quad \text{(A13)}$$

$$a_3(\gamma) = \cos\gamma L\sinh\gamma L - \sin\gamma L\cosh\gamma L \quad \text{(A14)}$$

while the position-dependent terms are:

$$f_1(x, \gamma) = \sin\gamma x + \sinh\gamma x \quad \text{(A15)}$$

$$f_2(x, \gamma) = \sin\gamma x - \sinh\gamma x \quad \text{(A16)}$$

$$f_3(x, \gamma) = \cos\gamma x - \cosh\gamma x \quad \text{(A17)}$$